Proceedings of the 20th International Conference on Soil Mechanics and Geotechnical Engineering– Rahman and Jaksa (Eds)

Effect of anisotropic creep on the convergence of deep drifts in Callovo-Oxfordian claystone

Effet de l'anisotropie de fluage sur la convergence des tunnels excavés en profondeur dans l'argilite du Callovo-Oxfordian

Sophie Jung & Amade Pouya & Siavash Ghabezloo
Laboratoire Navier, Ecole des Ponts ParisTech, France, sophie.jung@enpc.fr

Minh-Ngoc Vu
Andra, R&D Division, France

ABSTRACT: The French National Radioactive Waste Management Agency (ANDRA) is conducting a research program including in-situ experiments at the Meuse/Haute-Marne Underground Research Laboratory (MHM URL), which aims to demonstrate the feasibility of constructing and operating a deep geological radioactive waste disposal in the Callovo-Oxfordian (COx) claystone formation. A drift network of about 2km has been excavated essentially following minor and major horizontal stress directions in the MHM URL since 2000. Continuous monitoring shows that the convergence of the drifts has not stabilized yet, but the convergence rate decreases with time. Moreover, the convergence response strongly depends on the drift orientation. Understanding the time dependent behavior of the host rock is the key issue for optimizing the design of the disposal. This paper aims to present a constitutive model including threefold anisotropies (elasticity, plasticity and viscosity) to describe the behavior of COx claystone, with a focus on the time dependent behavior. Transverse isotropic elasticity is considered. Anisotropic Mohr-Coulomb criterion with perfect plasticity is used to represent the plastic behavior of the host rock. Anisotropic Lemaitre creep law is proposed to model the time dependent behavior of the COx claystone. Anisotropy is elaborated by introducing an equivalent stress tensor. Model parameters are calibrated based on laboratory tests on sample scale and then adjusted against the field observation in MHM URL. The proposed model is finally applied for modelling the anisotropic convergence observed in the drift GCS which is excavated in the direction of the major principal horizontal stress.

RÉSUMÉ : L'Agence nationale pour la gestion des déchets radioactifs (ANDRA) mène un programme de recherche comprenant des expériences in situ au Laboratoire de recherche souterrain de Meuse/Haute-Marne (URL MHM), qui vise à démontrer la faisabilité de la construction et de l'exploitation d'un stockage de déchets radioactifs en couche géologique profonde dans la formation argileuse du Callovo-Oxfordien (COx). Depuis 2000, un réseau de galeries d'environ 2 km a été creusé en suivant essentiellement les directions des contraintes horizontales mineures et majeures dans l'URL MHM. La surveillance continue montre que la convergence des galeries ne s'est pas encore stabilisée, mais que le taux de convergence diminue avec le temps. De plus, la convergence dépend fortement de l'orientation dans laquelle la galerie est excavée. La compréhension du comportement de la roche hôte en fonction du temps est un élément clé pour optimiser la conception des galeries d'enfouissement de déchets radioactifs. Cet article a pour but de présenter un modèle constitutif incluant trois anisotropies (élasticité, plasticité et viscosité) pour décrire le comportement de la roche argileuse, en mettant l'accent sur le comportement dépendant du temps. L'élasticité isotrope transversale est considérée. Le critère anisotrope de Mohr-Coulomb avec une plasticité parfaite est utilisé pour représenter le comportement plastique de la roche hôte. Une loi de fluage anisotrope suivant la loi de Lemaitre est proposée pour modéliser le comportement en fonction du temps du COx. L'anisotropie est élaborée en introduisant un tenseur de contraintes équivalent. Les paramètres du modèle sont calibrés sur la base de tests en laboratoire à l'échelle de l'échantillon, puis ajustés par rapport aux observations de terrain dans l'URL MHM. Le modèle proposé est finalement appliqué pour modéliser la convergence anisotrope observée dans la galerie GCS qui est excavée dans la direction de la contrainte horizontale principale majeure.

KEYWORDS: creep anisotropy, deep tunnel, convergence, COx claystone.

1 INTRODUCTION

Clay formations seem to present, in their natural undisturbed state, a very interesting environment for nuclear waste storage due to their confinement properties: low permeability, low diffusion coefficients and good retention capacity for radionuclides. Nevertheless, the excavation of the galleries induces a stress redistribution which leads generally to the creation of a damaged zone. This damaged zone has different mechanical and hydraulic properties compared to the undisturbed rock and its effects on the global behavior of the rock formation around the drifts should be taken into account. The fracturing pattern that is induced by the excavation of drifts in clay rock formation is a complex problem to study by itself. Theoretically, as mentioned by Labiouse and Vietor (2014), it is expected that in any bedded rock exhibiting an anisotropic (transversely isotropic) behavior, a circular hole is deformed into an overall oval shaped hole, with its principal axes parallel and orthogonal to the bedding planes, even if the far field stress would be isotropic. The difficulty is that when observations are made in two different bedded rocks (Opalinus Clay and Boom Clay), for the same mechanical conditions, the damaged zone is developing in reverse direction. This observation seems to indicate two different modes of failure in these two clays. Shear failure along conjugated planes seems, in the plastic Boom Clay, to result in a damaged zone extending in the horizontal direction. While bedding plane splitting and buckling occur in the indurated Opalinus Clay resulting in a damaged zone extending in the vertical direction (Labiouse and Vietor, 2014). Moreover, when it comes to COx claystone, which is the rock investigated in this paper, even though it is a hard and indurated rock more like Opalinus Clay, a fracture pattern similar to that observed in Boom Clay is observed for drifts and micro-tunnels parallel to the major horizontal stress (e.g. GCS drift) (Armand et al., 2014).

This shows the complexity of the mechanisms leading to the fracture pattern in the excavation damaged zone.

To demonstrate the feasibility of an industrial radioactive waste repository in deep geological formation, the French Radioactive Waste Management Agency (ANDRA) has built since 2000 an Underground Research Laboratory located in Meuse/Haute-Marne (MHM URL), where many experiments are being conducted. The MHM URL was mostly excavated in the Callovo-Oxfordian claystone (COx) found between 420 and 550m below the ground level. The argillaceous rock has been extensively studied over the past few years (Armand et al., 2017).

Continuous monitoring of the excavation zone around the drifts, has shown the development of an asymmetrical fractured zone around the drifts, with extensional and shear fractures (Armand et al., 2014). The directions of the convergence anisotropy and the geometry of the fractured zone depend on the direction of the drift with respect to the principal horizontal stresses.

For more than 10 years, modeling the hydro-mechanical responses to the excavation of two drifts of the MHM URL (GED and GCS drifts), has been the interest of several numerical research teams. A benchmark exercise supervised by ANDRA provides an overall view of the modeling related to the field observations (Seyedi et al., 2017). Modeling based on both discrete element (Yao et al., 2017) and continuum mechanic (Manica et al., 2017; Pardoen et al., 2015; Pardoen and Collin, 2017; Souley et al., 2017; Trivellato et al., 2019) approaches have been considered. Isotropic elasto-visco-plastic models have been adapted to reproduce the observation around the drift GED but failed in the case of GCS drift (Souley et al., 2017). Inherent anisotropy in plasticity or weakness planes have been usually necessary to model the anisotropic responses both in the excavation damage zone, and in the convergence (Manica et al., 2017; Pardoen et al., 2015; Pardoen and Collin, 2017). Moreover, in order to succeed in modeling the in situ observed convergences and damaged zone, the hydro-mechanical coupling and advanced numerical models have to be introduced, such as non-local model (Manica et al., 2018), and second gradient regularization (Pardoen and Collin, 2017). GCS drift presents an anisotropic convergence, despite its quasi isotropic stress state in its cross section. The anisotropic creep behavior has also been shown by Liu et al. (2015). However, the anisotropy in viscosity has not been taken into account in the previous constitutive models.

The aim of this work is to model the mechanical behavior of the rock formation containing the fractured zone around GCS drift, and mainly its viscous behavior, as observed in convergence monitoring of the drifts, in the after-excavation periods. The modeling of the viscous behavior of the rock mass around the drift is important for design of drifts to ensure their long-term integrity and performances. The development of the fractured zone around the drift during excavation process is beyond the scope of this work and we will focus on providing a time-dependent model allowing an efficient design of the lining support by taking into account the long term rock/lining interaction. As a matter of fact, the convergences of the drifts have to be well reproduced and extrapolated to long time periods in order to estimate the pressures applied by the drift convergence on the lining. We present a homogeneous and continuous model of the rock formation, without an explicit consideration of the fractures, that can reproduce the observed convergences in drifts in a purely mechanical simulation by using an elasto-visco-plastic law with three anisotropies in elasticity, plasticity and viscosity. We focus in reproducing the long term anisotropic convergences resulted from the anisotropic viscous behavior of the fractured zone with its specific directions.

2 DESCRIPTION OF THE GCS DRIFT

GCS drift was excavated along the major principal horizontal stress at the main level of the MHM URL. The state of stress in its cross section is rather isotropic with $\sigma_v = -12.7$MPa and $\sigma_h = -12.4$MPa. The drift was excavated with a road header, and its sections are circular with a 2.6m radius. The fractured zone expands essentially in the horizontal direction by 0.9 times the diameter of the excavation (Figure 1) (Armand et al., 2014). Its extension is more limited in the vertical direction, and reaches less than 0.1 diameter. There is a connected fractured zone where both extensional and shear fractures coexist. The extent of this zone is about 0.3 diameter from the drift wall in the horizontal direction. Beyond the connected fracture zone, there are only shear fractures. Figure 1 presents the convergence measurements at six instrumented sections, showing a bigger horizontal convergence than the vertical one.

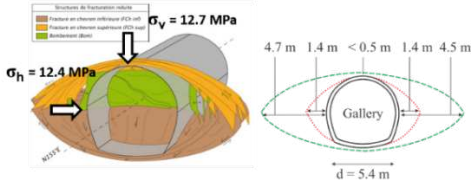

Figure 1. Conceptual model of GCS: Figure taken from (Armand, 2014)

3 CONSTITUTIVE MODEL ANELVIP

Two dimensional plain strain numerical simulations have been performed using the FEM code Disroc (Pouya, 2016). The cross-anisotropic elasto-viscoplastic model ANELVIP is used to simulate the behavior of the rock. The equations defining this constitutive model, as presented in Disroc Catalog of Materials (Fracsima, 2016), are described here for their general framework and in the following sections, for their elastic, plastic and viscous deformation components. As it is customary in infinitesimal strain constitutive models, the total strain rate is decomposed in three, elastic, plastic and viscous components as follows:

$$\dot{\boldsymbol{\varepsilon}} = \dot{\boldsymbol{\varepsilon}}^e + \dot{\boldsymbol{\varepsilon}}^p + \dot{\boldsymbol{\varepsilon}}^v \tag{1}$$

The mathematical expressions for the elastic, plastic and creep strains are given below:

$$\dot{\boldsymbol{\varepsilon}}^e = \mathbb{C}^{-1} : \dot{\boldsymbol{\sigma}} \tag{2}$$

$$F(\boldsymbol{\sigma}) < 0;\ \dot{\boldsymbol{\varepsilon}}^p = \dot{\lambda}\frac{\partial G}{\partial \boldsymbol{\sigma}} \tag{3}$$

$$\dot{\boldsymbol{\varepsilon}}^v = \psi(\sigma, \xi) \tag{4}$$

where $\mathbb{C}$ is the elastic tensor with transverse isotropy. F is the Mohr-Coulomb yield surface, G is the plastic potential which is chosen equal to F assuming an associated flow rule and $\dot{\lambda}$ is the plastic multiplier, and with the standard plastic flow rule conditions: $\dot{\lambda} \geq 0$; and $\dot{\lambda} = 0$ if $F(\boldsymbol{\sigma}) < 0$ or if $F(\boldsymbol{\sigma}) = 0$ and $\frac{\partial F}{\partial \boldsymbol{\sigma}}\dot{\sigma} < 0$. The function ψ corresponds to an anisotropic Lemaitre creep law with ξ the strain hardening parameter.

3.1 *Transverse isotropic elasticity*

The elastic behavior is transverse isotropic, with five parameters to be determined: two Young's moduli, two Poisson's ratio and one shear modulus. In the case of transverse isotropy around the y-axis, perpendicular to the plane of isotropy, we denote $E_y = E_\perp$ (perpendicular to the plane of isotropy) and the two

Young's moduli parallel to the plane of isotropy become equal $E_x = E_{\parallel}$.

The numerical values of the parameters come from experimental campaigns. As a matter of fact, Braun (2020) has shown that the anisotropy ratio between vertical and horizontal Young's moduli tends toward a constant value between 1.6 and 1.8. The following numerical values are considered: $E_x = E_{\parallel}$ = 5000 MPa, $E_y = E_{\perp}$ = 3000 MPa, υ_{yx}=0.3, υ_{xz}=0.2 and G = 1700 MPa. The shear modulus and the Poisson's ratios come from Guayacan-Carrillo et al. (2017).

3.2 *Plastic and viscous anisotropies*

The viscoplastic anisotropy in ANELVIP is built by replacing the stress tensor $\boldsymbol{\sigma}$ by a modified tensor $\tilde{\boldsymbol{\sigma}}$ obtained by a linear transformation of $\boldsymbol{\sigma}$. This is a classical method of defining anisotropic nonlinear materials used in plasticity first by Hill (1948) and more recently, only for plasticity, by Barlat et al. (2012) and by Mànica et al. (2017).

This linear transformation is defined, in a specific coordinates system, by the following relation:

$$\tilde{\boldsymbol{\sigma}} = \begin{bmatrix} \sigma_{xx} & f_T\sigma_{xy} & 0 \\ f_T\sigma_{xy} & f_N\sigma_{yy} & 0 \\ 0 & 0 & \sigma_{zz} \end{bmatrix} \tag{5}$$

This makes the constitutive model anisotropic and the coefficients f_N and f_T are determined in a way to obtain the desired anisotropy ratios. This relation is defined in a coordinate system (X,Y) making an angle ω with the reference system of coordinates allowing to specify the principal directions of anisotropy. The anisotropy ratio is then expressed preferentially by two parameters a_N and b_T related to the coefficients f_N and f_T by:

$$f_N = 1 + a_N \tag{6}$$

$$f_T = \sqrt{f_N + b_T} \tag{7}$$

The parameters a_N and b_T express the deviation from the isotropy; a_N=0 and b_T =0 correspond to the isotropic material. We define two pairs of parameters (a_N^p, b_T^p) and (a_N^v, b_T^v) respectively for the anisotropy of the plastic and viscous behavior. Using this method, we can transform an isotropic Mohr-Coulomb strength criterion to an anisotropic one by replacing the stress $\boldsymbol{\sigma}$ by the transformed stress $\tilde{\boldsymbol{\sigma}}$. In this anisotropic model, one can define the anisotropy function β^p as the ratio of the UCS (Uniaxial Compressive Strength) in any direction with respect to a reference direction, as can be seen in equation 10. This function depends on the parameters (a_N^p, b_T^p) with the expressions given by equations 10 and 11. Taking into account the symmetries of the material, this function can be defined only for $\bar{\theta}$ between 0° and 90°.

In the same way, one can transform a creep law for an isotropic material to an anisotropic one by replacing the stress by the transformed stress. Considering that the creep law is based on the Von Mises equivalent stress, one can define a function β^v, (equation 12) as the ratio of the transformed Von Mises equivalent stress to the non-transformed one for uniaxial stress in different directions. Note that $\sigma_e = \sqrt{\frac{3}{2}S_{ij}S_{ij}}$ with $S_{ij} = \sigma_{ij} - \frac{1}{3}\sigma_{kk}\delta_{ij}$. The expression of the function β^v depends on the parameters (a_N^v, b_T^v) and is given by the equation 12. The functions β^p and β^v are always equal to 1 for the reference direction $\bar{\theta}$ = 0°.

We need to know their values only for two other directions to determine the two parameters of anisotropy, a_N and b_T.

Their values for $\bar{\theta}$=90° allow determining the parameters a_N^v and a_N^p easily from $\beta(90°) = 1 + a_N$. Some examples of the anisotropy functions β^p and β^v are given in Figure 2. for different value of a_N and b_T to demonstrate how different situations of anisotropy can be reproduced by varying the values of these parameters. If both parameter a_N and b_T are zero, the isotropic behavior is recovered and the functions β describe a circle. A value of $a_N > 0$ (respectively $a_N < 0$) results in a value of β at $\bar{\theta}$=90° greater (respectively smaller) than 1. For the case of plasticity, a value of $b_T^p > 0$ (respectively $b_T^p < 0$) results in a maximum (respectively minimum) value of the function β^p at $\bar{\theta}$=45°.

$$\bar{\theta} = \theta - \omega \tag{8}$$

$$UCS(\bar{\theta}) = \frac{UCS(0°)}{\beta^p(\bar{\theta})} \tag{9}$$

For $b_T > 0$:

$$\beta^p(\bar{\theta}) = \frac{\sqrt{(1+a_N^p sin^2\bar{\theta})^2 + 4b_T^p sin^2\bar{\theta} cos^2\bar{\theta}} - (1+a_N^p sin^2\bar{\theta})sin\phi}{1 - sin\phi} \tag{10}$$

For $b_T < 0$:

$$\beta^p(\bar{\theta}) = \frac{1}{2}(1 + a_N^p sin^2\bar{\theta}\sqrt{\left(1 + a_N^p sin^2\bar{\theta}\right)^2 + 4b_T^p sin^2\bar{\theta} cos^2\bar{\theta}}) \tag{11}$$

$$\beta^v = \frac{\tilde{\sigma}_e}{\sigma_e} \tag{12}$$

$$\beta^v(\bar{\theta}) = \sqrt{(1 + a_N^v sin^2\bar{\theta})^2 + 3b_T^v sin^2\bar{\theta} cos^2\bar{\theta}} \tag{13}$$

In our model, the direction of anisotropy is given by the orientation of the principal fractures around the considered drift. Based on observations of the in situ fractured zones in GED and GCS drifts, we have considered that the shear fractures are mainly horizontal in the case of GED drift, while they are mainly vertical in the case of GCS drift. This is schematically presented in Figure 3. Of course, in reality the shear fractures are not plane, but in a first approximation, we consider that their global effect can be represented by a fractured material with some dominant direction of plane fractures. This assumption allows us to take into account the effects of the fractures forming the damaged zone on the drifts convergence, only by using a transverse isotropic model. In other words, we work with a homogeneous and continuous transverse isotropic material which represents the "homogenized" mechanical properties of a fractured rock mass with parallel horizontal or vertical fractures as schematized in Figure 3. The advantage of this approach is its simplicity, permitting to reproduce the convergence of both drifts, GED and GCS, only by changing the orientation of anisotropy: $\omega = 0°$ for the mostly horizontal fractures around GED drift, and $\omega = 90°$ for the mostly vertical fractures around GCS drift. The parameters of anisotropy are not the same for the two drifts since the density and the extent of the fractured zones are not the same. In this paper we focus on presenting the results of GCS drift.

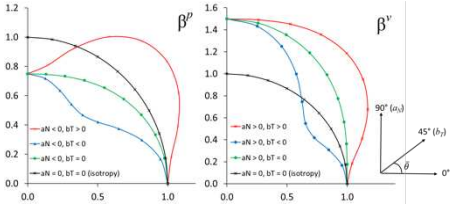

Figure 2. Representation of β^p and β^v in the polar coordinate system for different values of a_N^p, b_T^p, a_N^v and b_T^v.

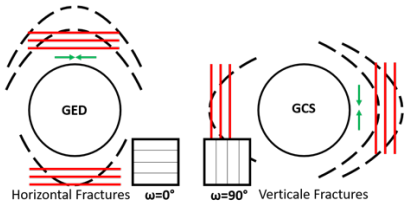

Figure 3. Schematic representation of the direction of the fractures (black) and of the dominant direction of fractures anisotropy (red) in the case of GCS drift. The green arrows represent the hoop stress at the vicinity of the drifts applied in the direction of reference.

3.3 *Anisotropic Mohr-Coulomb plasticity*

An anisotropic Mohr-Coulomb perfectly plastic yield function is used to model the plastic behavior of COx.

$$F(\tilde{\boldsymbol{\sigma}}) = \frac{\tilde{\sigma}_3 - \tilde{\sigma}_1}{2} + \frac{\tilde{\sigma}_3 + \tilde{\sigma}_1}{2} sin\phi - Ccos\phi \leq 0 \quad (14)$$

where C and ϕ are the cohesion and friction angle respectively. $\tilde{\sigma}_1$ and $\tilde{\sigma}_3$ are the major and minor principal stresses calculated from the transformed stress $\tilde{\boldsymbol{\sigma}}$. More sophisticated plastic criteria than Mohr-Coulomb have been considered in other works, but because the main objective of this paper is to analyze the anisotropic time-dependent effects, a simple plastic model was on purpose considered. However, the plastic behavior of the material determines the state of stress immediately after excavation and in this way influences the development of the viscous strain field. The UCS given by equation 9 depends on the direction in which the load is applied with regard to the fractures. Negative values of parameter b_T^p allows us to take into account the fact that the UCS is minimum when the load is applied at more or less 45° to the fractures. The strength parameters, cohesion and friction angle have been taken accordingly to the values stipulated in ANDRA's documents, with C = 5 MPa and ϕ = 24°. The plastic strain field is controlled by checking the short term convergences. As a matter of fact, Guayacan-Carrillo et al. (2017), succeeded in separating the instantaneous response to the excavation process from the time dependent one, making it possible to calibrate the elasto-plastic parameters of the constitutive law on the short term response of the claystone.

3.4 *Anisotropic Lemaitre creep law*

The expression of Lemaitre creep law called also the strain hardening law for an uniaxial stress state, neglecting the anisotropic effects, is the following:

$$\varepsilon(t) = a\langle\sigma - \sigma_c\rangle^n t^\alpha \quad (15)$$

The constitutive law depends on four parameters: a, n, σ_c and α. The parameter a is related to the magnitude of viscous strain, n is making the viscous strain nonlinear as a function of the stress, σ_c is the stress threshold for time-dependent deformations. To determine σ_c by laboratory tests, small stresses must be applied to the sample to see below which limit there is no more creep. This limit has not been studied by laboratory experiments for COx claystone. Another way to assess this threshold is to consider that the in situ stresses existing in the geological layers provide an upper bound of this threshold because it can be assumed that these layers have remained in the same creep free state for millions of years. By this reasoning, we get σ_c equal to the Mises equivalent stress for the in situ stresses which is about 3.6 MPa at the MHM URL location. The parameter α indicates the strain hardening in the creep law, with 0<α<1, as it can be seen in the equation (15), the smaller it is, the smaller the viscous strain rate is going to be. If $\alpha = 1$, the Norton-Hoff model, the model without strain hardening is retrieved.

In the ANELVIP model, the general form of the viscous deformation rate is expressed by:

$$\dot{\boldsymbol{\varepsilon}}^v = \frac{3}{2}\alpha\xi^{\alpha-1}\dot{\xi}\frac{\tilde{\boldsymbol{S}}^v}{\tilde{\sigma}_e^v} \quad (16)$$

$$\dot{\xi} = [a\beta^v\langle\tilde{\sigma}_e^p - \sigma_c\rangle^n]^{1/\alpha} \quad (17)$$

with $\tilde{\sigma}_e$ the Von-Mises equivalent stress $\tilde{\sigma}_e = \sqrt{\frac{3}{2}\tilde{S}_{ij}\tilde{S}_{ij}}$ with $\tilde{S}_{ij} = \tilde{\sigma}_{ij} - \frac{1}{3}\tilde{\sigma}_{kk}\delta_{ij}$. The tilde is referring to the transformation operated on the stress tensor making the model anisotropic, as explained in equation (5). We note $\tilde{\sigma}_e^v = \beta^v\tilde{\sigma}_e$ and $\tilde{\sigma}_e^p = \beta^p\tilde{\sigma}_e$. The function $\langle x\rangle$ is defined as:

$$\langle x\rangle = \begin{cases} 0 \; if \; x < 0 \\ 1 \; if \; x \geq 0 \end{cases} \quad (18)$$

Besides, to avoid numerical problems near $\xi = 0$, this law is completed by: $\dot{\boldsymbol{\varepsilon}}^v = \frac{3}{2}\alpha{\varepsilon_0}^{\alpha-1}\dot{\xi}\frac{\tilde{\boldsymbol{S}}^v}{\tilde{\sigma}_e^v}$ if $\xi^\alpha \leq \varepsilon_0$ where ε_0 is a small valued parameter introduced to avoid errors related to the division by zero. The transformed stresses in equation (16), $\tilde{\sigma}_e, \tilde{\boldsymbol{S}}^v, \tilde{\sigma}_e^v$ are defined by a transformation with parameters (a_N^v, b_T^v) as explained in section 3.1. Two different β functions are related to the anisotropy of viscous strains rate and the anisotropy of stress threshold for viscous strain, namely β^v and β^p respectively. The equation (19) can thus be written, function of the non transformed stress as:

$$\dot{\xi} = [a\beta^v(\bar{\theta})\langle\beta^p(\bar{\theta})\sigma_e - \sigma_c\rangle^n]^{1/\alpha} \quad (19)$$

Going back to the viscous law considered in ANELVIP, if the uniaxial stress $\sigma_{\bar{\theta}}$ is applied in a direction making an angle $\bar{\theta}$ with respect to x_1 (parallel to the fracture planes) then the axial creep strain measured in this direction is given by:

$$\varepsilon_{\bar{\theta}}(t) = a\beta^v(\bar{\theta})\langle\beta^p(\bar{\theta})\sigma_{\bar{\theta}} - \sigma_c\rangle^n t^\alpha \quad (20)$$

The six parameters governing the viscous behavior of the material, a, n, α, a_N^v, b_T^v and σ_c are first fitted on experimental data on the intact rock. The three parameters a, n, α of Lemaitre's creep law are fitted on a triaxial creep test provided by ANDRA. These parameters are fitted supposing an isotropic viscous behavior of the rock. As a matter of fact the anisotropy in viscosity is carried by the functions β^p and β^v and not by the parameters a, n, α and σ_c. The tests are conducted under a confining pressure of 12 MPa, while applying 50%, 75% and 90% of the peak stress, resulting in three curves giving axial strain evolution with time. The calibration is done by performing a linear regression with multiple parameters after linearizing Lemaitre creep law equation (21), allowing to determine the time dependency parameter α. Indeed, the first linear regression gives us $\ln(a) + nln(\sigma - \sigma_c)$ and α for the three different loadings. The parameter α is taken as an average value supposing that it does not depends on the stress.

$$\ln(\varepsilon) = \ln(a) + nln(\sigma - \sigma_c) + \alpha\ln(t) \quad (21)$$

As we know the numerical value of $\ln(a) + nln(\sigma - \sigma_c)$ and $ln(\sigma - \sigma_c)$, performing another linear regression on loading's to 50%, 75% and 90% of the peak stress, allows us to determine the two other parameters of the law, a and n. The results of the linear regressions are given in Figure 4.

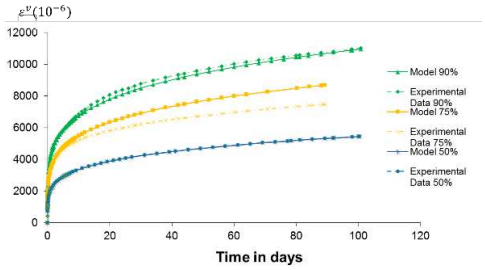

Figure 4. Axial viscoplastic strain for creep tests performed at 50, 75 and 90% of the peak strength. Experimental and numerical results.

4 NUMERICAL MODEL OF THE CONVERGENCE

As explained, the main idea of this work is to assume that the mechanical model of the rock, in which GCS drift is excavated, can be represented by that of a medium containing a family of parallel fractures. The orientation of these fractures corresponds to the dominant orientation in the fractured zone (Figure 3.) which develops during the excavation of the drifts. The "homogenized" mechanical behavior of this fractured medium can then be reasonably represented by a transverse isotropic behavior. Three different anisotropies, elastic, plastic and viscous, are taken into account based on the in-situ convergence measurements and the available knowledge on the rock's behavior. 2D plane strain simulations were performed using the finite element code Disroc (Pouya, 2016).

4.1 *Identification of anisotropy parameters*

The basic model parameters for the elastic, plastic and viscous parts have been evaluated based on the available experimental results on intact rocks and presented in section 3. It is assumed that the anisotropy is induced only by the fractured zone, and the effect of the intrinsic anisotropy of COx claystone (the bedding planes) on the orientation of the anisotropy is negligible in comparison to the effect of the fractured zone. The anisotropy parameters related to the plastic and the viscous deformations, $(a_N^p,\ b_T^p)$ and $(a_N^v,\ b_T^v)$ need to be calibrated through a simulation of the drift's convergence and comparison with in in situ measurements in GCS drift. In this way, the effect of the fractured zone around the drift will be indirectly taken into account in the calibrated values of the parameters. The calibrated model can then be used to extrapolate the drift's convergence to longer time periods.

Before doing the numerical simulations some first estimations of the anisotropy parameters have been obtained based on the available experimental results on the intact rock samples. Even though we consider that the effect of the fractured zone on the anisotropy is much more important than the intrinsic anisotropy of the rock, however, the estimations based on experimental results can be considered as starting points, probably lower bonds, of the calibration procedure.

The numerical simulations are compared with field measurements. Two convergence measurement strings that were installed during the drift excavation. Moreover, an extensometer has been emplaced from an adjacent drift in order to measure the rock displacement not only at the drift wall, but also in the rock at 0.78, 1.82, 3.38, 4.68, and 5.72 meters away from the drift wall. The set of model parameters are presented in table 1.

Table 1. Numerical values of the parameters used for the simulation of GCS drift.

Elasticity	Plasticity	Viscosity	Anisotropy
$E_{\parallel} = 5000\text{MPa}$	$C = 5\text{MPa}$	$a = 1.95 \times 10^{-4}$	$\omega = 90°$
$E_{\perp} = 3000\text{MPa}$	$\phi = 24°$	$n = 1$	$a_N^p = -0.25$
$\nu_{xy} = 0.3$	$\psi = 24°$	$\alpha = 0.215$	$b_T^p = 2.75$
$\nu_{xz} = 0.2$		$\sigma_c = 3.6\ \text{MPa}$	$a_N^v = 0.43$
G= 1700MPa			$b_T^v = -0.3$

In the case of GCS drift the identified anisotropy parameters for plasticity are a_N^p= -0.25 and b_T^p= 2.75. The negative value of a_N^p ensures that for the fractured rock the value of UCS in direction perpendicular to the fractures is greater than its value in direction parallel to the fractures. Moreover, the parameter a_N^p also controls the viscous stress threshold. For the anisotropy in viscous stress threshold, $a_N^p < 0$ means that the viscous strains start to develop for a smaller stress in the fractured rock than in the sound rock. With $b_T^p > a_N^p$, the UCS of the fractured rock is minimum when the load is applied at about 45° of the fracture plan. The calibrated functions β^p for GCS drift with their corresponding UCS are presented in Figure 5.

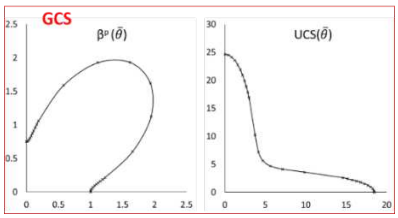

Figure 5. Polar representation of the functions β^p and UCS for GCS drift with a_N^p = -0.25 and b_T^p= 2.75

The calibrated function β^v is given in Figure 6.

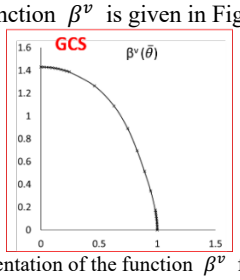

Figure 6. Polar representation of the function β^v for GCS drift with a_N^v = 0.43 and b_T^v= -0.3.

The numerical simulation results are presented in the next section and permit to verify the model ability to reproduce the observed drift's convergence and its anisotropy.

4.2 *Convergence simulation results*

We present first the simulated convergence for GCS drift in Figure 7. using the calibrated parameters as given in Table 1. One can see that the drift's convergence and its anisotropy show a quite good compatibility with in-situ measurements.

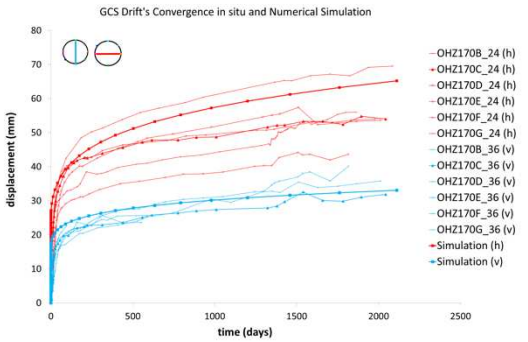

Figure 7. Comparison between in situ measurements and our numerical model.

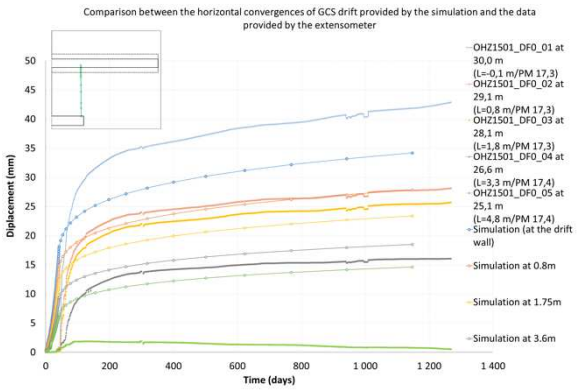

Figure 8. Comparison between the measurements of the extensometer and our numerical model.

Figure 7 shows a good reproduction of both vertical and horizontal convergences in GCS drift. The anisotropy in viscosity enable us to simulate anisotropic convergences rates in the two different directions. Nonetheless, Figure 8. shows that the model tends to overestimate the displacements outside the fractured zone as shown in green curve. This is not surprising, since by using a transverse isotropic model for the whole rock medium, there is no differentiation between the fractured zone and the sound rock. This is not critical as we only need the displacements at the drift wall to estimate the stresses in the linings.

5 CONCLUSIONS

To recall the objective of this work: it is to reproduce the convergence of the GCS drift with a continuous and homogeneous but anisotropic model. The anisotropic constitutive law will thus represent the global behavior of the rock mass around the drift, which is made of both sound rock and fractured rock in the fractured zone. The effect of the fractured zone on the convergence are taken into account with a threefold, elasto-visco-plastic, anisotropy. While the simplicity of the model does not permit to explain the creation of the fractured zone around the drifts itself, our goal is to enable a trustworthy reproduction of the rock formation after the excavation, and especially the time-dependent convergences due to the creep. This is essential to be able to provide a tool for the design of the lining supports based on the long term behavior of the drifts. We have introduced both viscous strain rate and viscous stress threshold anisotropy in the creep law, which allow us to get a more accurate response of the rock to the stress field for its viscous deformation. Moreover, as our viscous model takes into account a stress threshold, the stresses in the linings predicted by our model should be more realistic than the models considering the rock as a viscous fluid (without stress threshold).

The presented modeling approach allows us to take the fractured zone into account in a reasonably simple manner, without needing a precise knowledge of the fracture density or orientations in the fractured zones around the drifts to calibrate the parameters.

The model will also be applied to the GED drift, by considering that in this case the fractures are now horizontal, when they were vertical in the case of GCS drift. For this “new” transverse isotropic material, only the anisotropic parameters are going to be modified, otherwise the parameters (Young’s moduli, Poisson’s ratios, cohesion, friction angle etc.) remain the same.

6 REFERENCES

Armand, G., Conil, N., Talandier, J., Seyedi, D.M., 2017. Fundamental aspects of the hydromechanical behaviour of Callovo-Oxfordian claystone: From experimental studies to model calibration and validation. Computers and Geotechnics doi:10.1016/j.compgeo.2016.06.003.

Armand, G., Leveau, F., Nussbaum, C., De La Vaissiere, R., Noiret, A., Jaeggi,D., Landrein, P., Righini, C., 2014. Geometry and properties of the excavation-induced fractures at the meuse/haute-marne URL drifts. Rock Mechanics and Rock Engineering 47, 21–41. doi:10.1007/s00603-012-0339-6.

Barla, G., Debernardi, D., Sterpi, D., 2012. Time-Dependent Modeling of Tunnels in Squeezing Conditions. International Journal of Geomechanics 12, 697–710. doi:10.1061/(asce)gm.1943-5622.0000163.

Braun, P., Ghabezloo, S., Delage, P., 2020. Transversely isotropic poroelastic behaviour of the Callovo-Oxfordian claystone: A set of stress-dependent parameters. Rock Mechanics and Rock Engineering, 6–8 2020

Fracsima, 2016. Materials’ Catalogue.

Guayacan-Carrillo, L.M., Ghabezloo, S., Sulem, J., Seyedi, D.M., Armand, G., 2017. Effect of anisotropy and hydro-mechanical couplings on pore pressure evolution during tunnel excavation in low-permeability ground. International Journal of Rock Mechanics and Mining Sciences 97, 1–14. doi:10.1016/j.ijrmms.2017.02.016.

Guayacan-Carrillo, L.M., Sulem, J., Seyedi, D.M., Ghabezloo, S., Noiret, A., Armand, G., 2016. Analysis of Long-Term Anisotropic Convergence in Drifts Excavated in Callovo-Oxfordian Claystone. Rock Mechanics and Rock Engineering 49, 97–114. doi:10.1007/s00603-015-0737-7

Hill, R., 1948. A Theory of the Yielding and Plastic Flow of Anisotropic Metals. Series A, Mathematical and Physical Sciences 193, 281–297.

Labiouse, V., Vietor, T., 2014. Laboratory and in situ simulation tests of the excavation damaged zone around galleries in opalinus clay. Rock Mechanicsand Rock Engineering 47, 57–70. doi:10.1007/s00603-013-0389-4.

Lemaitre, J., 1971. Sur la détermination des lois de comportement des matériaux élastovisco-plastiques. Ph.D. thesis.

Liu, Z.B., Xie, S.Y., Shao, J.F., Conil, N., 2015. Effects of deviatoric stress and structural anisotropy on compressive creep behavior of a clayey rock. Applied Clay Science 114, 491–496. doi:10.1016/j.clay.2015.06.039.

Manica, M., Gens, A., Vaunat, J., Ruiz, D.F., 2017. A time-dependent anisotropic model for argillaceous rocks. Application to an underground excavation in Callovo-Oxfordian claystone. Computers and Geotechnics 85, 341–350. doi:10.1016/j.compgeo.2016.11.004.

Manica, M.A., Gens, A., Vaunat, J., Ruiz, D.F., 2018. Nonlocal plasticity modelling of strain localisation in stiff clays. Computers and Geotechnics 103,138–150. doi:10.1016/j.compgeo.2018.07.008.

Pardoen, B., Collin, F., 2017. Modelling the influence of strain localisation and viscosity on the behaviour of underground drifts drilled in claystone. Computers and Geotechnics 85, 351–367. doi:10.1016/j.compgeo.2016.05.017.

Pardoen, B., Levasseur, S., Collin, F., 2015. Using Local Second Gradient Model and Shear Strain Localisation to Model the Excavation Damaged Zone in Unsaturated Claystone. Rock Mechanics and Rock Engineering 48, 691–714. doi:10.1007/s00603-014-0580-2.

Pouya, A., 2016. Fracsima: Disroc, a Finite Element Code for modelling Thermo-Hydro-Mechanical processes in fractured porous media. URL:http://www.fracsima.com/DISROC.

Seyedi, D.M., Armand, G., Noiret, A., 2017. “Transverse Action” – A model benchmark exercise for numerical analysis of the Callovo-Oxfordian claystone hydromechanical response to excavation operations. Computers and Geotechnics 85, 287–305. doi:10.1016/j.compgeo.2016.08.008.

Souley, M., Armand, G., Kazmierczak, J.B., 2017. Hydro-elasto-viscoplastic modeling of a drift at the Meuse/Haute-Marne underground research laboratoratory (URL). Computers and Geotechnics 85, 306–320. doi:10.1016/j.compgeo.2016.12.012.

Trivellato, E., Pouya, A., Vu, M.N., Seyedi, D.M., 2019. A softening damage-based model for the failure zone around deep tunnels in quasi-brittle claystone, in: Peila, V..C.E. (Ed.), Tunnels and Underground Cities: Engineering and In-novation meet Archaeology, Architecture and Art- Proceedings of the WTC2019 ITA-AITES World Tunnel Congress. CRC Press.. May, pp. 4242–4251.doi:10.1201/9780429424441-449.